Fluid-solid interaction in the rate-dependent failure of brain tissue and biomimicking gels

M. Terzano[a,*], A. Spagnoli[a], D. Dini[b], A. E. Forte[c,d]

[a] *Department of Engineering and Architecture, University of Parma, Parco Area delle Scienze 181/A, 43124 Parma, Italy*
[b] *Department of Mechanical Engineering, Imperial College London, Exhibition Road, London SW7 2AZ, UK*
[c] *DEIB, Politecnico di Milano, Via Ponzio, 34/5 - 20133 Milano, Italy*
[d] *School of Engineering and Applied Sciences, Harvard University, Cambridge, Massachusetts, USA*

Abstract

Brain tissue is a heterogeneous material, constituted by a soft matrix filled with cerebrospinal fluid. The interactions between, and the complexity of each of these components are responsible for the non-linear rate-dependent behaviour that characterizes what is one of the most complex tissue in nature. Here, we investigate the influence of the cutting rate on the fracture properties of brain, through wire cutting experiments. We also present a computational model for the rate-dependent behaviour of fracture propagation in soft materials, which comprises the effects of fluid interaction through a poro-hyperelastic formulation. The method is developed in the framework of finite strain continuum mechanics, implemented in a commercial finite element code, and applied to the case of an edge-crack remotely loaded by a controlled displacement. Experimental and numerical results both show a toughening effect with increasing rates, which is linked to the energy dissipated by the fluid-solid interactions in the region surrounding the crack tip.

Keywords: brain tissue; hydrogels; rate-dependent fracture; poroelasticity

*Corresponding author. Tel.: +39-0521-905927; fax: +39-0521-905924;
e-mail: spagnoli@unipr.it.

March 2, 2021

1. Introduction

Brain tissue is arguably one of the most complex, delicate and heterogeneous tissues of the human body. Its structure is characterised by two main constituents: the grey matter, which contains the nerve cell bodies, and the white matter, with a large proportion of myelinated axons. By a mechanical point of view, neural tissues are among the softest of all internal organs, receiving protection from the skull and isolation from external actions by the cerebrospinal fluid (Budday et al., 2020). A large proportion of this fluid is free to move by diffusion and consolidation within the tissue's solid network; as a result, the brain behaves as a soft sponge: its microstructure, albeit highly inhomogeneous, presents small pores that are saturated by fluid (Forte et al., 2017). Diffusion has a fundamental importance for the brain function, delivering vital nutrients to the neural cells and playing an essential role in therapies based on drug delivery (Nicholson, 2001). Besides, the motion of fluid within the solid network causes volumetric shrinking and triggers consolidation effects (Franceschini et al., 2006), which can explain various phenomena, including the onset and evolution of hydrocephalus and the brain shift during surgeries (Forte et al., 2018). The interaction between interstitial fluid and solid matrix provides a source of energy dissipation, which results in time-dependent behaviour frequently observed during mechanical testing (Jin et al., 2013; Forte et al., 2017). In addition, a further source of dissipation is related to viscoelasticity, caused by intracellular interactions between cytoplasm, nucleus and the cell membrane (Budday et al., 2017a).

Mechanical models of the brain tissue at the continuum scale are usually formulated in the framework of finite strain mechanics, addressing the nonlinear elastic and time-dependent behaviour (de Rooij and Kuhl, 2016). The biphasic nature of the tissue can be captured by models derived from the classical theory of consolidation in soil mechanics (Franceschini et al., 2006), eventually coupled with large deformations (Forte et al., 2017; Hosseini-Farid et al., 2020). An equivalent description has been developed in the context of mixture theories, leading to the formulation of a consistent framework for soft porous media (Ehlers and Eipper, 1999; Comellas et al., 2020). Time-dependent behaviour due to viscous effects

has been described by generalised Maxwell models or more refined descriptions elaborated in the finite strain theory (Budday et al., 2017b; Haldar and Pal, 2018). However, with respect to tissue failure, our understanding is considerably more limited. It is known that the brain tissue, as most internal organs, does not carry significant mechanical loads; nevertheless, traumatic injuries expose the tissue to damage and fracture (El Sayed et al., 2008). Furthermore, the tissue can be perforated with catheters, needles and probes, during minimally invasive surgeries and regenerative therapeutics (Ashammakhi et al., 2019; Terzano et al., 2020). Due to its high heterogeneity, failure properties in the brain tissue are region dependent. In the white matter, which is characterized by fibrous axonal structures, failure occurs by tearing of fibres when the tissue is loaded above a certain threshold (Budday et al., 2020). At the microscale, axonal injury involves a viscoelastic mechanism with stretching and sliding of microtubules, depending on the entity of the deformation (Cloots et al., 2011). While the contribution of fluid-solid interaction in terms of the tissue mechanical behaviour is widely recognised, the role of fluid diffusion during failure has not been investigated. Furthermore, the flow of fluid in the brain tissue is not homogeneous (Jamal et al., 2020). Due to the different microstructure, white matter is far more permeable than grey matter, which instead presents densely connected networks that can entrap the fluid phase (Budday et al., 2020). Such a difference might explain the stronger rate-dependency of white matter during compression and tensile tests, because of a faster fluid drainage (Budday et al., 2020). However, the characteristic time of fluid draining depends on the size of the perturbed region, which also makes this contribution dependent on testing conditions (Wang and Hong, 2012). Therefore, there is a need for investigating how rate-dependency and fluid-structure interactions affect fracture propagation in brain tissue.

When a porous network is filled or saturated with fluid, mechanical and hydraulic responses are coupled: forces and deformations change the pressure of interstitial fluid, while pressure gradients drive fluid flow, resulting in mechanical deformation. During fracture, the flow of fluid inside the crack-tip zone might affect the surface energy required for crack initiation and propagation. Despite scarce information in the context of biological tissues, illuminating evidences come from experimental work on failure of

hydrogels. As an example, studies on reversible gels suggest that the fracture energy can be increased by the drainage of fluid in the crack-tip zone (Naassaoui et al., 2018).

In this work, our aim is to shed light on the rate-dependent fracture process in the brain tissue caused by fluid draining. Firstly, we present the results of fracture tests performed on porcine brain samples. To this aim we use the wire cutting protocol, which is a well established method to measure the fracture properties of soft materials, including viscous foodstuff and gels (Goh et al., 2005; Baldi et al., 2012; Forte et al., 2015). A computational model is then developed in the framework of finite strain continuum mechanics, representing the large strain behaviour and fluid interaction through a poro-hyperelastic model (Simon, 1992). The numerical analyses are focused on the process of crack propagation, which in the case of wire cutting develops after the initial stages of indentation and tissue rupture (Terzano, 2020). Through a simplified model of the fracture process in dissipative materials, we are able to consider the energy dissipated by fluid-structure interaction as a function of the loading rate. Finally, we provide a comparison with the poroelastic behaviour of a biomimicking gel that was previously characterised by Forte et al. (2015).

2. Materials and methods

2.1. Wire cutting tests

When measuring the fracture toughness of soft materials, traditional techniques based on stress intensity factors cannot be employed, since failure occurs when a large portion of the material is well beyond the limit of small strain elasticity. Toughness is hereby defined as the total amount of energy absorption during deformation until fracture occurs. Wire cutting tests were preferred with respect to other available methods (such as, for instance, edge-notched tensile tests) because of the issues related to the extreme softness of the brain tissue, the effect of self-weight and the impossibility of realising proper clamping. Porcine brain tissue samples were prepared, removing the cerebellum and separating the two hemispheres; each hemisphere was then positioned in the sample container with the frontal lobe facing

upwards. The specimen would slowly shift under gravity and approximately occupy a square prism of length 30 mm, width 30 mm and height 50mm. Steel wires of diameter $d_w = 0.05, 0.16, 0.25, 0.5$mm were inserted with an insertion speed of $v = 5\text{mm}\,\text{s}^{-1}$, and the test with $d_w = 0.16$mm was repeated with $v = 0.5\text{mm}\,\text{s}^{-1}$ and $v = 50\text{mm}\,\text{s}^{-1}$. All tests were performed with a Biomomentum Mach-1™mechanical testing system using a 1.5 N single-axis load cell, in a conditioned room at 19 °C temperature (Forte et al., 2016). A schematic of the experimental setup is shown in Fig.1.

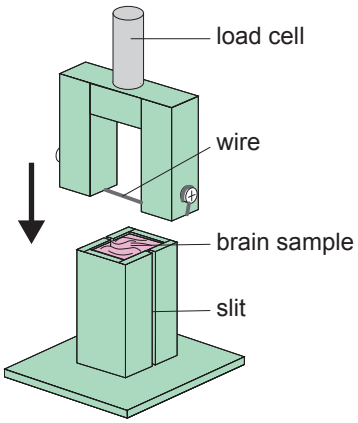

Figure 1. Wire cutting testing schematic. 1-col figure

2.2. Model of poroelastic fracture

A model is proposed to account for the rate-dependency observed during wire cutting tests on the porcine brain samples, which can be extended to similar materials with a soft and wet porous microstructure. It is based on the following assumptions: (i) brain tissue and the biomimicking gels are modelled as poro-hyperelastic materials; (ii) rate-dependent failure is described with a model of the fracture process based on the spatial separation of dissipative length scales and the definition of a cohesive process zone; (iii) fracture in cutting is assimilated to the propagation of a far-field loaded crack, depending on a geometric parameter (in this specific case, the wire diameter).

2.2.1. Poro-hyperelastic model

In this section, the brain tissue and the biomimicking gels are treated as biphasic soft materials, where a solid skeleton is saturated by biological fluids, and a poro-hyperelastic model is described, with specific focus on the equations needed for its numerical implementation in a finite element (FE) code (Forte et al., 2017). The theory of finite deformation continuum mechanics, as presented in standard textbooks on the subject, e.g. Holzapfel (2000), is the background on which the model is developed. Accordingly, a material point of the biphasic medium is identified in the current configuration by the position vector $\boldsymbol{x}(\boldsymbol{X},t)$, $\boldsymbol{u}_S \equiv \boldsymbol{u} = \boldsymbol{x} - \boldsymbol{X}(\boldsymbol{x},t)$ is the displacement of this point in the porous solid phase and $\boldsymbol{u}_F$ defines the corresponding quantity for the pore fluid (Simon, 1992) (Fig.2a). We also recall the decomposition of the spatial velocity gradient $\mathbf{l} = \nabla\dot{\boldsymbol{u}} = \mathbf{d} + \mathbf{w}$, where $\mathbf{d} = \mathrm{sym}(\nabla\dot{\boldsymbol{u}})$ is the symmetric rate of deformation tensor, $\mathbf{w} = -\mathbf{w}^T$ is the anti-symmetric spin tensor and $\dot{\boldsymbol{u}}$ is the velocity of the solid phase.[1]

In a biphasic material, each phase in the current configuration is defined by a volume fraction $n_\alpha = \mathrm{d}v_\alpha/\mathrm{d}v$, where $\alpha = S, F$ corresponds, respectively, to the solid skeleton and the pore fluid. Assuming conditions of saturation, we establish the fundamental relationship $n_F + n_S = 1$ (Cheng, 2016). In the following, we denote $n = n_F$ the porosity of the medium, which is correlated to the current void ratio through $e = n/(1-n)$. The continuity mass equation for phase α reads (Ehlers and Eipper, 1999)

$$\frac{\mathrm{D}}{\mathrm{D}t}(n_\alpha\rho_\alpha) + n_\alpha\rho_\alpha\nabla\cdot\dot{\boldsymbol{u}}_\alpha = 0 \tag{1}$$

where $\mathrm{D}(\bullet)/\mathrm{D}t$ is used for the material time derivative and ρ_α is the effective density of each phase. In the solid skeleton, Eq.(1) provides the following relationship

$$\frac{(1-n)}{(1-n_0)} = J_S J^{-1} \tag{2}$$

[1]Throughout this section, $\nabla(\bullet)$ denotes the spatial gradient while $\nabla\cdot(\bullet)$ is used for the spatial divergence operator. Italic is used for scalars, bold italic for vectors and bold roman for tensors.

where n_0 is the porosity in the initial configuration, J is the volume ratio of the biphasic material and J_S is instead referred to the solid skeleton. Notice that if the matrix is assumed incompressible, we have $J_S = 1$; however, this does not lead to macroscopic incompressibility, because volume change can occur through changes in the volume fractions. Considering an incompressible fluid phase, Eq.(1) can be rewritten as

$$\frac{\mathrm{D}}{\mathrm{D}t} n + n \nabla \cdot \dot{\boldsymbol{u}}_F = 0 \tag{3}$$

For consistency with an updated Lagrangian framework in which the incremental solution strategy is implemented in the commercial FE code adopted, field equations need to be referred to the current configuration. In particular, the weak form of the linear momentum balance involves the rate of the Cauchy stress tensor $\boldsymbol{\sigma}$, which is provided by (Holzapfel, 2000)

$$\dot{\boldsymbol{\sigma}} = \boldsymbol{\sigma}'^{J} + \mathbf{w} \cdot \boldsymbol{\sigma} + \boldsymbol{\sigma} \cdot \mathbf{w}^T - \dot{p_F} \mathbf{I} \tag{4}$$

where $\boldsymbol{\sigma}'^{J}$ is the Jaumann rate of the effective Cauchy stress, given by $\boldsymbol{\sigma}' = \boldsymbol{\sigma} + p_F \mathbf{I}$, with $p_F = -1/3 \, \mathrm{tr} \boldsymbol{\sigma}$ being the pore pressure and $\boldsymbol{I}$ the second-order identity tensor.

Finally, we introduce the constitutive assumptions for the biphasic medium. The fluid flow through the porous skeleton is characterized by Darcy's law, with an isotropic permeability tensor which remains unchanged during the deformation. Although formulated in the context of soil mechanics, Darcy's approach is consistently employed in modelling biological tissues, including brain and cartilage (Simon, 1992; Franceschini et al., 2006; Hosseini-Farid et al., 2020; Comellas et al., 2020). The phenomenon of swelling, related for instance to the absorption of fluid molecules by the solid network, is not considered in the model. In the macroscale description adopted in this work, the pore pressure appears to be a consistent variable to describe the energy dissipated by fluid-solid interactions. In quasi-static conditions

and neglecting inertia, Darcy's law correlates the rate of fluid volume to the pressure gradient

$$\dot{\boldsymbol{w}} = -\frac{\kappa}{\eta_F}\nabla p_F \tag{5}$$

where $\dot{\boldsymbol{w}} = n(\dot{\boldsymbol{u}}_F - \dot{\boldsymbol{u}})$ is the seepage velocity, representing the rate of fluid volume flowing through a unit normal area, κ is the intrinsic permeability and η_F is the fluid viscosity (Cheng, 2016).

The behaviour of the solid skeleton is specified by a hyperelastic isotropic strain energy function. Several studies related to brain mechanics, e.g. Budday et al. (2017a); Forte et al. (2017), have shown that a modified one-term Ogden model provides optimal fit to experimental data. The compressibility of the solid skeleton is implemented through the usual decomposition of the solid deformation into isochoric and volumetric parts, such that the strain energy density is provided by

$$\Psi(\bar{\lambda}_i) + U(J) = \frac{2\mu}{\alpha^2}\left(\bar{\lambda}_1^\alpha + \bar{\lambda}_2^\alpha + \bar{\lambda}_3^\alpha - 3\right) + \frac{1}{D}(J-1)^2 \tag{6}$$

where μ, α and $D = 2/K_S$ (K_S is the bulk modulus) are material parameters and $\bar{\lambda}_i = J^{-1/3}\lambda_i$ are the modified principal stretches (Holzapfel, 2000). The effective Cauchy stress tensor is split into its deviatoric and volumetric components $\boldsymbol{\sigma}' = \mathbf{s}' + p'\mathbf{I}$ (Selvadurai and Suvorov, 2016), with $p' = \partial U/\partial J$ and (Connolly et al., 2019)

$$\mathbf{s}' = J^{-1}\beta_i(\boldsymbol{n}_i \otimes \boldsymbol{n}_i) \tag{7}$$

where $\boldsymbol{n}_i$ are the principal spatial directions and the stress coefficients are expressed by $\beta_i = \bar{\lambda}_i\partial\Psi/\partial\bar{\lambda}_i - 1/3\bar{\lambda}_j\partial\Psi/\partial\bar{\lambda}_j$ (the summation rule applies to repeated indices). The last step required for the numerical implementation in the updated Lagrangian framework is to make explicit the objective rate introduced in Eq.(4) through a spatial fourth-order elasticity tensor, such that

$$\boldsymbol{\sigma}'^{J} = \mathbb{c}'_J : \mathbf{d} \tag{8}$$

where $\mathbb{c}'_J$ is the spatial elasticity tensor defined in terms of the Jaumann rate of the Cauchy stress. The explicit formulation for a compressible hyperelastic model in terms of the principal stretches can be found, for instance, in the recent work by Connolly et al. (2019). For completeness, we recall that a discretised and linearised form of the previous equations is needed, where variations are computed with respect to the field variables of the problem —which in our case are represented by nodal displacements $\boldsymbol{u}$ and pore pressure values p_F.

2.2.2. Rate-dependent fracture process

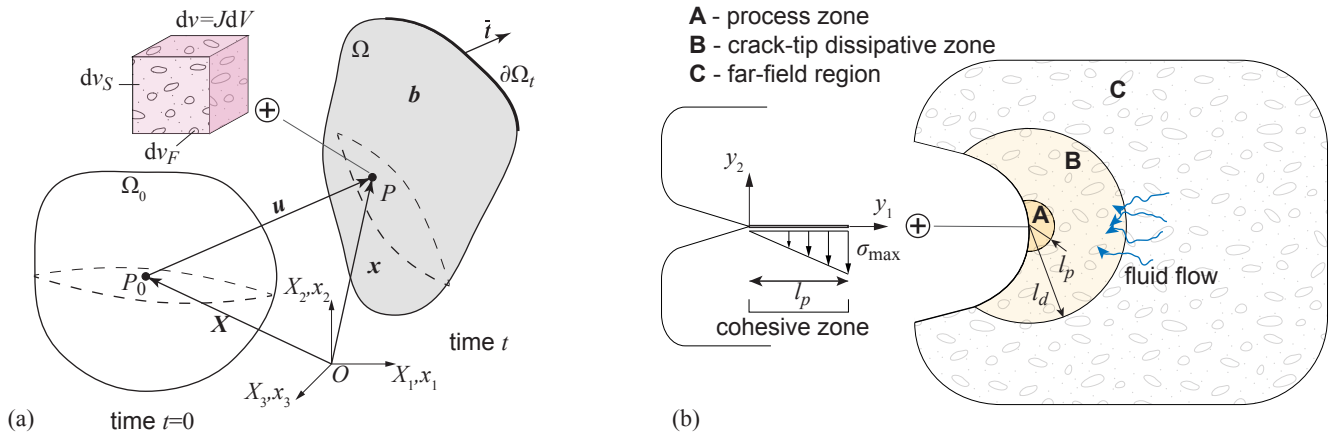

Figure 2. (a) Reference and current configurations of a biphasic continuum body. (b) Illustrative sketch of the fracture process in a poroelastic soft material. Shown in figure are (A) the process zone with radius l_p, (B) the crack-tip dissipative zone with radius l_d and (C) the far-field region. The enlarged view shows the process zone schematised with a rate-independent cohesive zone model. 2-col figure

The flow of interstitial fluid in the pores of a soft solid skeleton results in time-dependent deformation and draining of the biphasic medium, according to a relaxation time which depends on the material properties (namely, the permeability) and the length of macroscopic observation (Hu and Suo, 2012). Hence, the analysis of rate-dependent fracture requires that poroelastic relaxation is considered as a source of energy dissipation correlated to crack propagation, in which the length of observation is put in relation with some characteristic size of the fracture process. The model here proposed is based on the ideal case illustrated in Fig.2b, where a propagating crack in a semi-infinite body is shown with

three regions where dissipative phenomena possibly occur (Terzano, 2020). Firstly, we have damage phenomena occurring at the molecular scale, which are condensed within a process zone of radius l_p and account for the intrinsic toughness of the material. At a larger scale, dissipative terms are originated from relaxation in the bulk material but become relevant to crack propagation only if they affect the crack-tip region, which for now we broadly define as the material affected by the vicinity of the crack. Their effect is to prevent the crack driving force provided by external loading from being fully delivered to the crack. Finally, we have bulk relaxation processes in the far-field zone, which however might be neglected as they do not directly contribute to the fracture process.

As a consequence of the proposed decomposition, following Zhao (2014) we can split the fracture energy in two terms: the intrinsic term Γ_o originating from the process zone, and an additional term Γ_d due to energy dissipation in the crack-tip region affected by propagation

$$\Gamma = \Gamma_o + \Gamma_d \tag{9}$$

In our work, the intrinsic toughness Γ_o is considered rate-independent. Conceptually, this is equivalent to employ a cohesive process zone which enriches the continuum poro-hyperelastic model with a prescribed rate-independent stress-displacement relationship on the separation interface (Schwalbe et al., 2012) (see the enlarged view in Fig.2b). The term Γ_d includes energy dissipation due to the drainage of fluid in the crack-tip region, whose size l_d depends in general on a typical size of the specific test (Hu and Suo, 2012). In wire cutting the relevant length parameter is the radius of the wire; however, as explained in Sect. 2.2.3, we can formulate the hypothesis that the size of the dissipative crack-tip region is provided by the so-called elasto-adhesive length, which is a characteristic of the fracture process (Creton and Ciccotti, 2016). This length scale defines the concept of softness by a fracture mechanics point of view and represents the distance at which the energy cost of creating new crack surfaces is

comparable to the strain energy in the material. Therefore we may write

$$l_d = \Gamma_o / E \tag{10}$$

where E is the initial Young's modulus of the material and $l_d \gg l_p$ in order to ensure the separability of scales between the different regions. Please notice that Eq.(10) also provides, to a first approximation, a measure of the radius ϱ_o of a blunted crack in an elastic material (Creton and Ciccotti, 2016).

2.2.3. Fracture process in wire cutting

Cutting with wires involves deformation, friction and fracture in the target material. In this Section, we describe the approach through which we could describe the cutting process by focusing on crack propagation only. Frictional effects are neglected due to the reduced contact area of wires. Our aim is to establish the limits under which crack propagation in cutting can be compared to propagating a crack in symmetric far-field loading conditions (Fig.3).

Differently from crack propagation under remote loading, the finite size of the wire adds an additional length to the fracture process of cutting (Terzano et al., 2018). It is assumed that the tool exerts some sort of constraint on the elastic blunting of the crack, which can be limited by the fact that the crack opening displacement is determined by the tool geometry. By comparing the critical tip radius of a blunted crack ϱ_o, which is a material property, with the wire diameter d_w we are able to distinguish two different scenarios (Terzano, 2020):

- for $d_w \geq 2\varrho_o$, crack propagation happens as an autonomous process under symmetric mode-I conditions, with a certain distance between the wire and the crack tip. The crack tip radius is determined by its natural value ϱ_o, approximately defined by Eq.(10);
- for $d_w < 2\varrho_o$, the shape of the blunted crack is constrained by the wire, which touches the crack-tip. In this situation, the mechanism of propagation is different from that under remote loads and requires a further input of external energy. In other terms, crack propagation is energy limited.

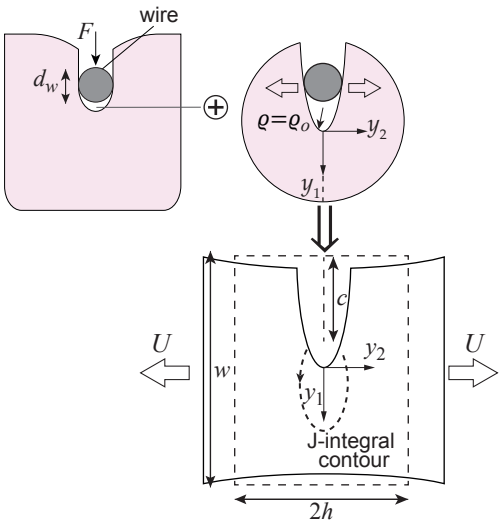

Figure 3. Sketch of the plane strain geometry employed to investigate the elastic fracture process in wire cutting. Under the assumption of $d_w \geq 2\varrho_o$, the equivalent model of an edge crack of length c, subjected to an opening remote displacement U, is obtained. The local system y_1, y_2 is defined with respect to the moving crack tip. 1-col figure

The analyses of rate-dependent fracture described in this work applies to wire cutting under the assumption that crack propagation is an autonomous process, that is, for $d_w \geq 2\varrho_o$. Although the previous criterion is derived in a purely elastic situation, we assume that it is extended to the biphasic material.

3. Results

3.1. Experimental

Force-displacement curves obtained from wire cutting tests on the porcine brain tissue are illustrated in Fig.4a, for a wire diameter $d_w = 0.16$mm and three insertion speeds (average of various tests). Following the initial indentation, in which the tissue deforms prior to fracture, the force tends to stabilise in the steady-state phase of cutting (Terzano et al., 2018). Differently from the results of similar tests on other soft materials (Forte et al., 2015), the transition to the steady state is not well marked in the brain tissue, due to the extreme softness and the inhomogeneous structure of the samples. In Fig.4b we

show the force-displacement curves for single tests, where one can distinguish two peaks, corresponding to grey and white matter failure, followed by relaxation, before reaching an approximately stable trait where the wire cuts through the sample.

Wire cutting can be employed to infer the intrinsic toughness of the tissue Γ_o. To do so, we need to remove the contribution due to energy dissipation; typically, this means performing a fracture test at very low loading rates, so that quasi-static conditions are assumed. The results are here elaborated according to the model proposed by Kamyab et al. (1998). Briefly, the steady-state cutting force F_{ss} results from the force needed to open the crack and a contribution due to the formation of a flow zone around the bottom half of the wire, as shown in Fig.4c. Friction produces a circumferential stress in this region but is neglected everywhere else. Then, the force per unit thickness is proportional to the wire diameter, according to

$$\frac{F_{ss}}{t} = \Gamma + (1+f)\,\sigma_{\max} d_w \tag{11}$$

where $\sigma_{\max}$ has to be intended as a characteristic cohesive stress of the material, f is the frictional coefficient and t is the out-of-plane thickness of the sample.

The steady-state force F_{ss}/t obtained from the cutting experiments at $v = 5\text{mm}\,\text{s}^{-1}$ is plotted as a function of the wire diameter in Fig.4d. Since a steady value cannot be easily recognised, F_{ss} is computed as the average force corresponding to the onset of crack propagation observed in the tests. A linear fit is employed to extrapolate the force to zero diameter, such that, according to Eq.(11), the value of the fracture toughness is obtained. However, data from the test performed at $v = 0.5\text{mm}\,\text{s}^{-1}$ show that the force F_{ss}/t is lower, suggesting that there might be an extra contribution due to energy dissipation resulting in $\Gamma > \Gamma_o$. Lacking complete data for lower velocities, due to the complexity of realising proper tests on the super-soft brain tissue, we then hypothesize that the same force-diameter slope applies to any insertion speed and employ the intercept at $d_w = 0.16$ mm to extrapolate the corresponding steady-state forces. These are shown on a logarithmic plane in Fig.4e and fitted with a linear interpolating function. The intercept with the vertical axis, corresponding to a quasi-static value

of the insertion speed, should provide the correct value of Γ_o. Furthermore, the increase of toughness with speed follows a power-law, with exponent approximately equal to 0.2. Due to the uncertainty in experimental data, we might assume that a value of Γ_o comprised between $0.1 - 1\mathrm{J\,m^{-2}}$ is a reasonable approximation. Indeed, this is the same order of magnitude of the toughness of biomimicking gelatins computed from wire cutting tests by Forte et al. (2015).

3.2. FE analyses

3.2.1. Fracture in the elastic material

Before employing FE analyses to understand the origin of the rate-dependent fracture properties observed in experiments, we need to verify the hypothesis presented in Sect.2.2.3, which allows us to reduce the cutting problem to one of crack propagation under remote loading when $d_w \geq 2\varrho_0$. To this purpose, we have modelled the steady-state cutting phase as the insertion of a rigid circular wire into an elastic edge-cracked body of width w and height $2h$, with initial crack length c (see Fig.3). Since the wire extension in the out-of-plane direction is much larger than the thickness t of the samples, a plain strain assumption is introduced. Due to symmetry, only half specimen is modelled with pertinent constraints imposed to the lower edge of the body. Eight-node plane strain elements are adopted, with a suitable refinement around the crack tip, which is artificially blunted by taking an initial small radius of curvature. From analyses of mesh convergence, the smallest element in the crack tip region is equal to $10^{-5}\,h$. The sample material is purely elastic, described by the strain energy provided in Eq.(6). In such a case, the crack driving energy can be computed through the J-integral, such that the onset of crack propagation occurs when $J_{\mathrm{int}} = \Gamma_o$. The parameters of the brain tissue implemented in the FE model are summarised in Table 1 (please notice that fluid-related quantities are not relevant here). The analyses were run with the quasi-static implicit solver of the commercial software Abaqus.

We have studied the insertion of wires with diameter $d_w = 0.125 - 1\,\mathrm{mm}$ that are pushed into the crack for its full length. According to the hypotheses presented in Sect.2.2.3, frictional effects are not considered; however, a small coefficient of Coulomb's friction was introduced in the FE analyses because

Table 1. Mechanical parameters of the poro-hyperelastic model

Ogden's parameters	Brain tissue [1]	Gelatin (10% w/w) [2]
μ (Pa)	$0.52 \cdot 10^3$	$6.21 \cdot 10^3$
α	-4.4	2.64
D Pa^{-1}	$1.3 \cdot 10^{-3}$	$69 \cdot 10^{-6}$
Hydraulic conductivity k $\mathrm{m\,s}^{-1}$	$1.57 \cdot 10^{-9}$	$1.25 \cdot 10^{-6}$
Fluid specific weight γ_F ($\mathrm{kN\,m}^{-3}$)	9741	9741
Initial void ratio e (%)	20	90
Intrinsic toughness Γ_o $\mathrm{J\,m}^{-2}$	0.1	1.1

[1] Forte et al. (2017)
[2] Forte et al. (2015)

we have found that it helped to achieve numerical convergence of the contact algorithm. From the deformed coordinates y_1, y_2, the radius of the blunted crack can be expressed through the radius ϱ of a circle fitting the profile within a distance equal to $10^{-3}c$ from the crack tip. Plots of the deformed crack when $J_{\mathrm{int}} = \Gamma_o$ are shown in Fig.5a, suggesting that the crack blunting with wires of various diameters is almost equivalent to the edge-crack subjected to remote loading. The case of an edge-crack subjected to far-field loading, by means of applied displacements U in the direction perpendicular to the crack, is added as comparison (dashed line in the plot). The crack profiles look very similar, except that corresponding to $d_w = 0.125$mm, which displays a markedly different trend. By plotting the critical crack tip radius ϱ against the wire diameter d_w for each case considered (Fig.5b), we notice that they are all approximately equal to a constant value. Interestingly, such a value is a good approximation of the characteristic length $\varrho_o = \Gamma_o/E$, which for the brain tissue is in the order of $0.65 \cdot 10^{-4}$m. Therefore, the transition to constrained blunting seems to occur when $d_w = 0.125$mm. Below this limit, we hypothesise that the tip radius scales with the wire diameter (hence the slope 1/2 shown in the plots). In conclusion, we can assume that, in the materials under consideration, steady-state cutting can be reduced to a problem of crack propagation when the wire diameter is $d_w \geq 0.13$mm.

3.2.2. Fracture in the biphasic medium

Retaining the assumption of autonomous crack propagation, we can study rate-dependent fracture in the equivalent edge-cracked model with applied remote displacements. The geometry is illustrated in Fig.6a: it consists of a large rectangular sample of width $2h = 50$mm and height $w = 20$mm, containing an edge-crack of length $c = 1$mm. Normal displacements are applied to the left and right boundaries such that the strain rate is constant, that is $U = [\exp(\dot{\varepsilon}t) - 1]\, h$, where $\varepsilon = \ln[(h + U)/h]$ is the true strain in the direction normal to the crack line. The stretch ratio is defined by $\lambda = 1 + U/h$. Two materials, the brain tissue and the gelatin studied by Forte et al. (2015), are described with the poro-hyperelastic model presented in Sect.2.2. The properties are summarised in Table 1. Notice that the hydraulic conductivity k is employed in place of the permeability κ, to which is related by means of $k = \kappa\gamma_F/\eta_F$. The finite element mesh is built with four-node quadrilateral plane strain hybrid elements with additional degrees of freedom for the pore pressure p_F. The smallest element in the crack tip region is equal to $10^{-5}\, h$. Boundary conditions are specified in terms of displacements (left and right edges are prevented from lateral motion), and in addition on the pore pressure degree of freedom. A condition of draining, enforced by setting the pore pressure equal to zero, is specified for the horizontal free edges and the edge-crack surfaces in contact with atmospheric pressure (Fig.6a). The reference porosity n_0 needs to be specified as initial condition through the void ratio e. The analyses were run with the implicit solver of the commercial software Abaqus. A transient fluid-stress diffusion analysis is required to simulate fluid flow through the porous material, where the accuracy of the solution is governed by the maximum pore pressure change allowed in an increment. Different values have been considered for the best compromise between accuracy and efficiency.

The main purpose of the analyses is to understand how fluid draining in the crack-tip region affects the onset of crack propagation. In other terms, we are considering the effect of dissipation and of the loading rate on the crack driving energy, whereas the fracture toughness is assumed equal to Γ_o. The

critical condition is then defined by

$$J_{\text{int}}(\dot{\varepsilon}) = \Gamma_o \tag{12}$$

Due to coupling between deformation of the solid network and fluid diffusion, the J-integral is path-dependent since it includes poroelastic dissipation. In the biphasic material its definition is provided by

$$J_{\text{int}} = \int_C \left(\Psi n_1 - \frac{\partial u_i}{\partial x_1} \sigma'_{ij} n_j \right) \mathrm{d}s, \tag{13}$$

where Ψ is the strain energy density and n_j is the unit vector normal to a contour C enclosing the crack tip (Fig.3). The results presented below are obtained considering a contour that surrounds the crack-tip dissipative zone, whose radius, from Eq.(10), is approximated to $l_d = 0.65 \cdot 10^{-4}$m.

A preliminary analysis on the elastic material is employed to investigate the quasi-static situation. In such a case, the critical condition evaluated through Eqs.(12)-(13) provides the stretch λ_o, corresponding to the onset of crack propagation. Results in the poroelastic materials are illustrated in Fig.6b, where we show the contours of the fluid pressure p_F, for three different strain rates $\dot{\varepsilon}$, when $\lambda = \lambda_o$, within the crack-tip dissipative zone. The red areas correspond to the drained or relaxed condition ($p_F = 0$) whereas the blue regions are affected by fluid flowing in the pores. It can be seen that, independently from the rate, the greater permeability of gelatins allows for a rapid draining of the whole crack-tip region. On the contrary, it appears that fluid takes a longer time to drain the same area in the brain tissue, where permeability is much lower. Since fluid draining is a dissipative process, it is reasonable to assume that crack propagation is affected by this phenomenon, at least in the brain tissue. In Fig.6c we present the normalised energy at constant stretch λ_o for different strain rates. The observed behaviour can be better comprehended by plotting the normalised stretch when $J_{\text{int}} = \Gamma_o$, Fig.6d. As expected, no difference with respect to the elastic quasi-static situation emerges in the gelatin, which therefore behaves as an elastic relaxed material. The situation looks different in the brain tissue, where both the strain energy and the critical stretch are affected by rate. Notice that we cannot consider these stretches as the real ultimate stretches of the material, since the J-integral does not provide an exact measure of

the crack driving energy; nevertheless, the results shown in Fig.6d suggest a toughening effect due to fluid draining in the brain tissue.

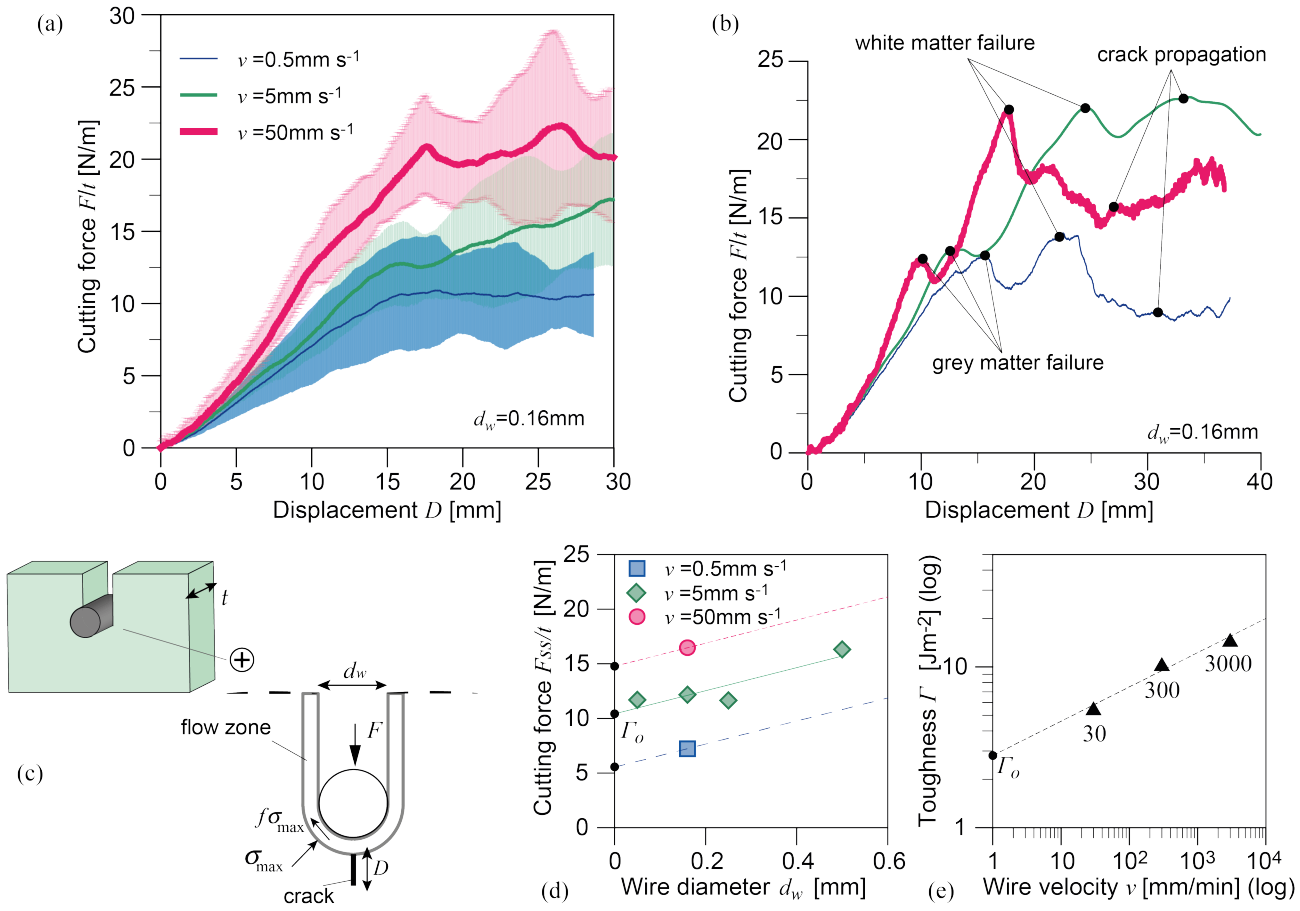

Figure 4. (a) Cutting force versus displacement for $d_w = 0.16$mm. The curves show the average of various tests on porcine brain tissue, with a high dispersion due to the inhomogeneous structure of the samples. (b) Force-displacement from single tests at the three different insertion speeds, showing the corresponding stages of material failure. (c) Schematic of wire cutting showing the model of the rupture process proposed by Kamyab et al. (1998). (d) Steady state force F_{ss}/t as a function of the wire diameter. The continuous linear fit is obtained for $v = 5\text{mms}^{-1}$. (e) Logarithmic plot of the intrinsic toughness as a function of the insertion speed. 2-col figure

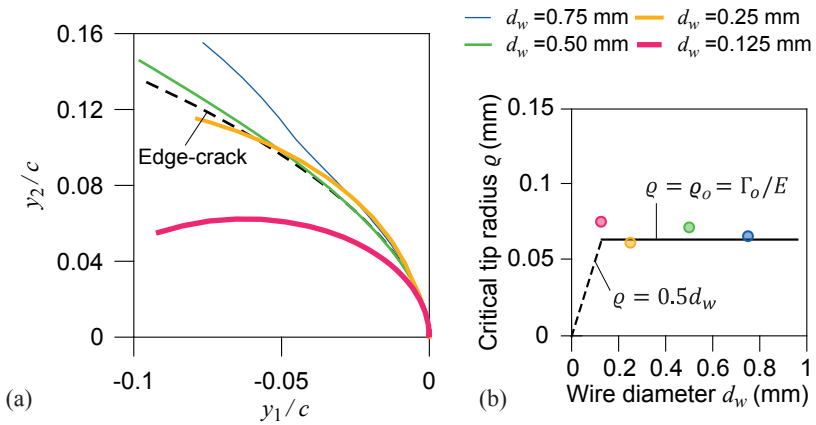

Figure 5. (a) Deformed crack profiles in the elastic brain tissue when $J = \Gamma_o$, for an edge-crack (dashed line) and different wire diameters d_w. (b) Corresponding crack tip radius ϱ versus the wire diameter. The horizontal line is the natural crack tip radius ϱ_o. 2-col figure

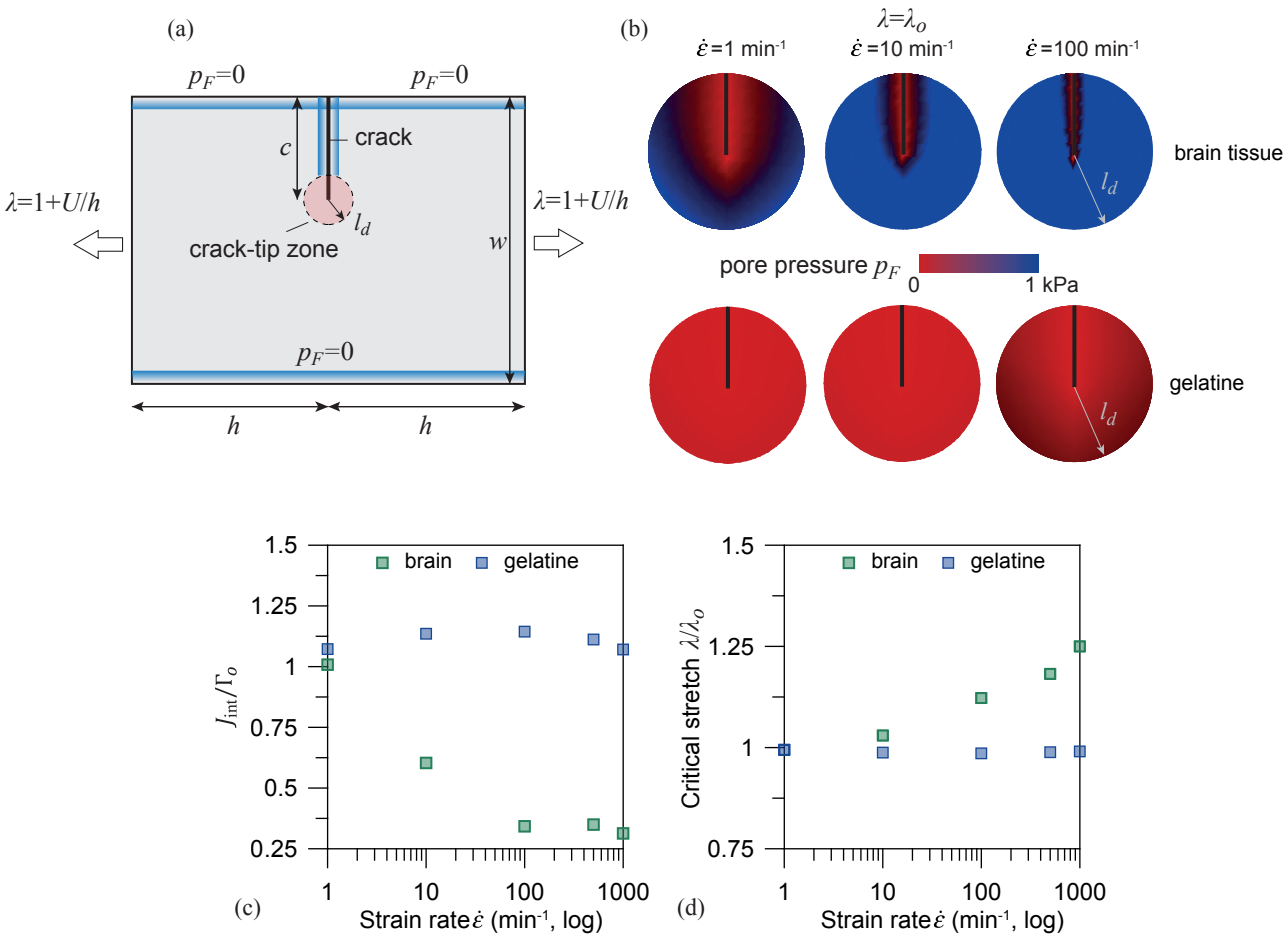

Figure 6. (a) Model of the edge-cracked sample for the analyses of poroelastic fracture. Light-blue edges are those with drained boundary conditions. (b) Contours of the pore pressure p_F at constant stretch $\lambda = \lambda_o$ for different strain rates, in the brain tissue and the gelatin studied by Forte et al. (2015). (c) Strain energy per unit area in the crack-tip region, normalised by the fracture toughness Γ_o, and (d) applied stretch, normalised by the critical stretch in quasi-static conditions λ_o. Both are plotted as a function of the strain rate $\dot{\varepsilon}$ (logarithmic plot). 2-col figure

4. Discussion

Both experimental and numerical results suggest that the fracture properties of the brain tissue are rate-dependent. Although we cannot rule out the effect of viscoelasticity, our study is focused on the effects of fluid draining in the biphasic medium. This phenomenon is often neglected in the analysis of fracture or other situations with relatively fast loading rates, based on the observation that poroelastic relaxation derives from a long-range motion of interstitial fluid in the solid network. Indeed, in macroscopic samples the process is quite slow compared, for instance, to viscoelastic relaxation (Hu and Suo, 2012). However, we point out that the characteristic time of poroelastic relaxation also depends on the characteristic length of observation, which in the presence of a crack is much smaller than the characteristic size of the sample. Since the topic of fracture in the brain tissue is not well documented, we can employ observations on fracture of hydrogels in order to discuss the results obtained.

In the crack-tip zone of soft porous tissues, high uniaxial tensile stresses trigger a take-up of fluid from the far-field region. Since these high stress gradients are confined to a small region, whose extension in the brain tissue under investigation is in the order of 10^{-5} m, fluid draining of the crack tip zone is a relatively quick phenomenon. The mechanism is illustrated in Fig.7: initially the solid is saturated and there is only an infinitesimal zone close to the tip of the existing crack where the fluid pressure is zero; as time goes by, this region increases in extent until the whole crack-tip region is drained. The key observation is that the draining process is relevant with respect to fracture only if the material relaxation in the crack-tip dissipative region happens in times comparable to those of crack propagation. By treating the pressure-driven fluid flow in the biphasic medium as a diffusive process, the time of poroelastic relaxation can be defined as the time needed to drain an area of radius l_d (Hui et al., 2013)

$$t_d = l_d^2 / D_F \tag{14}$$

where D_F is the diffusion coefficient, which depends on the permeability, the fluid viscosity and the elastic properties of the solid. To a first approximation, in linear poroelasticity and plane strain conditions we

have $D_F = 2\mu(1-\nu)\kappa/(1-2\nu)\eta_F$, where μ and ν are, respectively, the shear modulus and Poisson's ratio of the solid material. Ideally, we can distinguish two limit situations:

- slow strain rates or high permeability: the draining process extends to a large region surrounding the crack-tip zone. Here we observe an extended relaxation but this becomes ineffective with respect to fracture. The material behaves as a soft compressible solid;
- fast strain rates or reduced permeability: fluid diffusion is too slow to be effective and the crack-tip region is saturated at the instant corresponding to the onset of propagation. With respect to fracture, the material behaves as a soft incompressible solid.

Critical situations are those in the middle, where fluid draining may produce an enhancement of the material fracture toughness. This is the effect that we have observed with our model in the brain tissue (Fig.6). On the contrary, the case of gelatin falls in the situation of highly permeable materials. However, there are some limits in the procedure adopted, which deserve to be discussed below and will be addressed in future research.

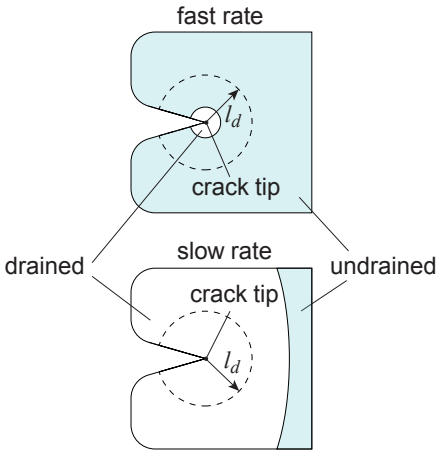

Figure 7. Sketch of the crack-tip dissipative region and influence of fluid draining at fast and slow strain rates $\dot{\varepsilon}$. 1-col figure

The computational model that we have proposed is based on the separation of length scales, with

the assumption that the process zone is rate-independent. Indeed, putting into relation its extension to the average spacing of the network, which is in the scale of 50-100 nanometers (Tønnesen et al., 2018; Vidotto et al., 2019), the hypothesis seems to be well motivated. However, other studies explained fluid-related toughening based on draining within the process zone: interestingly, Forte et al. (2015) proposed a mechanism of this type to justify the observed rate-dependent fracture properties of gelatin, which cannot be captured by the analyses presented in this work. Although the proposed poro-hyperelastic model is able to couple large deformation and fluid flow, more advanced models considering the full coupling between the solvent diffusion and tissue swelling might be required, e.g. Hong et al. (2008); Bouklas et al. (2015a); Brighenti and Cosma (2020). This would also allow us to implement a modified definition of the J-integral proposed for swelling materials, which is path-independent and computes the transient energy energy release rate by separating the energy lost in diffusion from the energy available to drive crack growth (Bouklas et al., 2015b).

The model of rate-dependent fracture was applied to analyse experimental data coming from wire cutting tests. We have explained, supported by dedicated numerical analyses (see Fig.5), the limits under which we can isolate the stage of crack propagation, leaving aside the whole process of contact and indentation that occurs in the experiments. Specifically, this happens above a critical wire diameter; below, crack propagation becomes unstable and the shape of the crack is constrained. This behaviour was also observed experimentally in hydrogels by other authors (Baldi et al., 2012) and motivated by the reduced stiffness of such materials. More correctly, we are able to say that it depends on the competition between the cost of creating new surfaces and the elastic strain energy of the material. Although our FE results provided meaningful insights on poroelastic toughening (Figs. 6c-d), we have no means to establish a direct confrontation with the experimental data. As a matter of fact, experiments revealed a rate-dependent toughening in terms of the velocity of wire insertion (Figs. 4e), which in the steady-state can be reasonably considered to coincide with the crack velocity. In the numerical model we have instead explored the effect of the strain rate on the onset of crack propagation, but we cannot establish an analytical relationship between the strain rate and the crack propagation velocity. It comes

naturally to think that higher strain rates result in faster crack propagation, although this might hold only below a certain limit, as shown for instance in fracture tests on hydrogels (Mayumi et al., 2016). Ideally, we could have simulated the complete cutting process directly through the finite element model and use cohesive elements to simulate the process of propagation. Incidentally, a similar approach has successfully modelled complex cutting problems in soft elastic materials (Terzano et al., 2020; Skamniotis and Charalambides, 2020). However, to calibrate the cohesive model for the brain tissue would have required additional data for the characterisation of its frictional behaviour, and possibly some effects of fluid lubrication (Reale and Dunn, 2017), which are unknown.

Finally, we discuss shortcomings of the method through which we have derived the intrinsic fracture toughness of brain tissue, in the order of $\Gamma_0 = 0.1 - 1 \mathrm{J\,m^{-2}}$. In Fig.4d we have assumed that the slope of the steady state cutting force F_{SS} versus the wire diameter d_w is the same for different velocities. However, wire cutting analyses on biomimicking gelatins by Forte et al. (2015) have shown that the slope of the interpolating function increases with the insertion velocity while it tends to become constant only at low velocities. Furthermore, the extrapolation procedure to infer the intrinsic toughness Γ_o from Eq.(11) was based on the assumption that $v = 1 \,\mathrm{mm\,min^{-1}}$ is a reasonable speed for quasi-static conditions. To a first approximation, we might relate the quasi-static threshold to the process of fluid diffusion, which in turn depends on the permeability of the material. The employed value was also derived from similar observations by Forte et al. (2015) on gelatins. However, considering the large difference with the permeability of brain tissue, our assumption needs to be verified against further experimental observations. This point brings us to a last aspect that should be considered in future work: the issue of accurately measuring and modelling permeability. For the sake of simplicity, we have adopted the hypothesis of material isotropy: however, while this seems to be a valid assumption for the elasticity of the brain tissue, diffusion or permeability properties are remarkably anisotropic, in particular in white matter regions characterised by axonal structures (Jamal et al., 2020). In addition, brain tissue permeability can be modified substantially under loading by swelling and additional coupling with the local tissue deformation, suggesting the need of more refined models.

5. Conclusion

Testing the fracture properties of super soft tissues through standard tensile specimens is a complex task. For this reason, wire cutting was here employed to analyse the influence of rate on the fracture energy of brain tissue. The experimental data show an evident increase of the cutting force with the rate of insertion, suggesting that some form of energy dissipation affects the cutting process. In this work, we speculate that the rate-dependent toughening is due to poroelastic dissipation in the vicinity of the crack that is propagated ahead of the wire. We have proposed a computational model which considers the brain tissue as a biphasic poro-hyperelastic material. Through finite elements analyses of an edge-cracked sample, subjected to remote loading with varying strain rate, we have shown how the process of fluid draining in the crack-tip region might affect the fracture toughness of the material. We can then summarise the main findings:

- the analysis of wire cutting experimental data suggests a power-law increase of fracture toughness with the rate of insertion, as already observed in biomimicking gelatins;
- we have identified a length scale which distinguishes the fracture process of cutting in soft materials from crack propagation under remote loading;
- finite element analyses of the fracture process in the poroelastic material have confirmed the toughening effect with the rate of applied loading. According to the poro-hyperelastic model, such a contribution is chiefly controlled by the value of the intrinsic permeability of the material.

This work has purposely neglected the dissipative behaviour provided by viscoelasticity in order to focus on fluid-related effects. Future work will be dedicated to extend the proposed model to coupled viscoelasticity and fluid diffusion. In the context of fracture, accurate models should specifically target the rate-sensitivity of the process zone. By a computational point of view, cohesive models might still be the ideal candidates to include energy dissipation through a time-dependent cohesive law. Our view is that they should be developed on the ground of a micromechanical description of the disintegrating

material ahead of the crack tip. In particular, we envisage that further research is needed to characterise the effect of water diffusion on mechanical deformation by a micromechanical point of view.

6. Acknowledgements

A. E. Forte acknowledges the support received from the European Union's Horizon 2020 research and innovation programme under the Marie Skłodowska-Curie grant agreement No 798244. The authors also acknowledge the financial support from EDEN2020 project funded by the European Union's Horizon 2020 research and innovation programme under grant agreement No 688279. D. Dini would like to acknowledge the support received from the UKRI Engineering and Physical Sciences Research Council (EPSRC) via his Established Career Fellowship EP/N025954/1.

References

Ashammakhi, N., Ahadian, S., Darabi, M.A., El Tahchi, M., Lee, J., Suthiwanich, K., Sheikhi, A., Dokmeci, M.R., Oklu, R., Khademhosseini, A., 2019. Minimally Invasive and Regenerative Therapeutics. Advanced Materials 31, 1804041. doi:10.1002/adma.201804041.

Baldi, F., Bignotti, F., Peroni, I., Agnelli, S., Riccò, T., 2012. On the measurement of the fracture resistance of polyacrylamide hydrogels by wire cutting tests. Polymer Testing 31, 455–465. doi:10.1016/j.polymertesting.2012.01.009.

Bouklas, N., Landis, C.M., Huang, R., 2015a. A nonlinear, transient finite element method for coupled solvent diffusion and large deformation of hydrogels. Journal of the Mechanics and Physics of Solids 79, 21–43. doi:10.1016/j.jmps.2015.03.004.

Bouklas, N., Landis, C.M., Huang, R., 2015b. Effect of Solvent Diffusion on Crack-Tip Fields and Driving Force for Fracture of Hydrogels. Journal of Applied Mechanics 82, 081007. doi:10.1115/1.4030587.

Brighenti, R., Cosma, M.P., 2020. Swelling mechanism in smart polymers responsive to mechano-chemical stimuli. Journal of the Mechanics and Physics of Solids 143, 104011. doi:10.1016/j.jmps.2020.104011.

Budday, S., Ovaert, T.C., Holzapfel, G.A., Steinmann, P., Kuhl, E., 2020. Fifty Shades of Brain: A Review on the Mechanical Testing and Modeling of Brain Tissue. Archives of Computational Methods in Engineering 27, 1187–1230. doi:10.1007/s11831-019-09352-w.

Budday, S., Sommer, G., Birkl, C., Langkammer, C., Haybaeck, J., Kohnert, J., Bauer, M., Paulsen, F., Steinmann, P., Kuhl, E., Holzapfel, G.A., 2017a. Mechanical characterization of human brain tissue. Acta Biomaterialia 48, 319–340. doi:10.1016/j.actbio.2016.10.036.

Budday, S., Sommer, G., Holzapfel, G.A., Steinmann, P., Kuhl, E., 2017b. Viscoelastic parameter identification of human brain tissue. Journal of the Mechanical Behavior of Biomedical Materials 74, 463–476. doi:10.1016/j.jmbbm.2017.07.014.

Cheng, A.H.D., 2016. Poroelasticity. Theory and Applications of Transport in Porous Media, Springer International Publishing, New York.

Cloots, R.J.H., van Dommelen, J.A.W., Nyberg, T., Kleiven, S., Geers, M.G.D., 2011. Micromechanics of diffuse axonal injury: influence of axonal orientation and anisotropy. Biomechanics and Modeling in Mechanobiology 10, 413–422. doi:10.1007/s10237-010-0243-5.

Comellas, E., Budday, S., Pelteret, J.P., Holzapfel, G.A., Steinmann, P., 2020. Modeling the porous and viscous responses of human brain tissue behavior. Computer Methods in Applied Mechanics and Engineering 369, 113128. doi:10.1016/j.cma.2020.113128.

Connolly, S.J., Mackenzie, D., Gorash, Y., 2019. Isotropic hyperelasticity in principal stretches: explicit elasticity tensors and numerical implementation. Computational Mechanics 64, 1273–1288. doi:10.1007/s00466-019-01707-1.

Creton, C., Ciccotti, M., 2016. Fracture and adhesion of soft materials: a review. Reports on Progress in Physics 79, 046601. doi:10.1088/0034-4885/79/4/046601.

Ehlers, W., Eipper, G., 1999. Finite Elastic Deformations in Liquid-Saturated and Empty Porous Solids, in: Porous Media: Theory and Experiments. Springer Netherlands, Dordrecht. volume 34, pp. 179–191.

El Sayed, T., Mota, A., Fraternali, F., Ortiz, M., 2008. Biomechanics of traumatic brain injury. Computer Methods in Applied Mechanics and Engineering 197, 4692–4701. doi:10.1016/j.cma.2008.06.006.

Forte, A.E., D'Amico, F., Charalambides, M.N., Dini, D., Williams, J.G., 2015. Modelling and experimental characterisation of the rate dependent fracture properties of gelatine gels. Food Hydrocolloids 46, 180–190. doi:10.1016/j.foodhyd.2014.12.028.

Forte, A.E., Galvan, S., Dini, D., 2018. Models and tissue mimics for brain shift simulations. Biomechanics and Modeling in Mechanobiology 17, 249–261. doi:10.1007/s10237-017-0958-7.

Forte, A.E., Galvan, S., Manieri, F., Rodriguez y Baena, F., Dini, D., 2016. A composite hydrogel for brain tissue phantoms. Materials & Design 112, 227–238. doi:10.1016/j.matdes.2016.09.063.

Forte, A.E., Gentleman, S.M., Dini, D., 2017. On the characterization of the heterogeneous mechanical response of human brain tissue. Biomechanics and Modeling in Mechanobiology 16, 907–920. doi:10.1007/s10237-016-0860-8.

Franceschini, G., Bigoni, D., Regitnig, P., Holzapfel, G.A., 2006. Brain tissue deforms similarly to filled elastomers and follows consolidation theory. Journal of the Mechanics and Physics of Solids 54, 2592–2620. doi:10.1016/j.jmps.2006.05.004.

Goh, S.M., Charalambides, M.N., Williams, J.G., 2005. On the mechanics of wire cutting of cheese. Engineering Fracture Mechanics 72, 931–946. doi:10.1016/j.engfracmech.2004.07.015.

Haldar, K., Pal, C., 2018. Rate dependent anisotropic constitutive modeling of brain tissue undergoing large deformation. Journal of the Mechanical Behavior of Biomedical Materials 81, 178–194. doi:10.1016/j.jmbbm.2017.12.021.

Holzapfel, G.A., 2000. Nonlinear Solid Mechanics: A Continuum Approach for Engineering Science. Wiley, Chichester.

Hong, W., Zhao, X., Zhou, J., Suo, Z., 2008. A theory of coupled diffusion and large deformation in polymeric gels. Journal of the Mechanics and Physics of Solids 56, 1779–1793. doi:10.1016/j.jmps.2007.11.010.

Hosseini-Farid, M., Ramzanpour, M., McLean, J., Ziejewski, M., Karami, G., 2020. A poro-hyper-viscoelastic rate-dependent constitutive modeling for the analysis of brain tissues. Journal of the Mechanical Behavior of Biomedical Materials 102, 103475. doi:10.1016/j.jmbbm.2019.103475.

Hu, Y., Suo, Z., 2012. Viscoelasticity and poroelasticity in elastomeric gels. Acta Mechanica Solida Sinica 25, 441–458. doi:10.1016/S0894-9166(12)60039-1.

Hui, C.Y., Long, R., Ning, J., 2013. Stress Relaxation Near the Tip of a Stationary Mode I Crack in a Poroelastic Solid. Journal of Applied Mechanics 80. doi:10.1115/1.4007228.

Jamal, A., Mongelli, M.T., Vidotto, M., Madekurozwa, M., Bernardini, A., Overby, D.R., De Momi, E., Rodriguez y Baena, F., Sherwood, J.M., Dini, D., 2020. Infusion Mechanisms in Brain White Matter and its Dependence of Microstructure: An Experimental Study of Hydraulic Permeability. IEEE Transactions on Biomedical Engineering doi:10.1109/TBME.2020.3024117.

Jin, X., Zhu, F., Mao, H., Ming, S., Yang, K.H., 2013. A comprehensive experimental study on material properties of human brain tissue. Journal of Biomechanics 46, 2795–801. doi:10.1016/j.jbiomech.2013.09.001.

Kamyab, I., Chakrabarti, S., Williams, J.G., 1998. Cutting cheese with wire. Journal of Materials Science 33, 2763–2770. doi:10.1023/A:1017517332112.

Mayumi, K., Guo, J., Narita, T., Hui, C.Y., Creton, C., 2016. Fracture of dual crosslink gels with permanent and transient crosslinks. Extreme Mechanics Letters 6, 52–59. doi:10.1016/j.eml.2015.12.002.

Naassaoui, I., Ronsin, O., Baumberger, T., 2018. A poroelastic signature of the dry/wet state of a crack tip propagating steadily in a physical hydrogel. Extreme Mechanics Letters 22, 8–12. doi:10.1016/j.eml.2018.04.004.

Nicholson, C., 2001. Diffusion and related transport mechanisms in brain tissue. Reports on Progress in Physics 64, 815–884. doi:10.1088/0034-4885/64/7/202.

Reale, E.R., Dunn, A.C., 2017. Poroelasticity-driven lubrication in hydrogel interfaces. Soft Matter 13, 428–435. doi:10.1039/C6SM02111E.

de Rooij, R., Kuhl, E., 2016. Constitutive Modeling of Brain Tissue: Current Perspectives. Applied Mechanics Reviews 68, 010801. doi:10.1115/1.4032436.

Schwalbe, K.H., Scheider, I., Cornec, A., 2012. Guidelines for Applying Cohesive Models to the Damage Behaviour of Engineering Materials and Structures. Springer, Heidelberg.

Selvadurai, A.P., Suvorov, A.P., 2016. Coupled hydro-mechanical effects in a poro-hyperelastic material. Journal of the Mechanics and Physics of Solids 91, 311–333. doi:10.1016/j.jmps.2016.03.005.

Simon, B.R., 1992. Multiphase Poroelastic Finite Element Models for Soft Tissue Structures. Applied Mechanics Reviews 45, 191–218. doi:10.1115/1.3121397.

Skamniotis, C., Charalambides, M.N., 2020. Development of computational design tools for characterising and modelling cutting in ultra soft solids. Extreme Mechanics Letters 40, 100964. doi:10.1016/j.eml.2020.100964.

Terzano, M., 2020. Fracture processes in indentation and cutting of soft biomaterials. Phd thesis. University of Parma.

Terzano, M., Dini, D., Rodriguez y Baena, F., Spagnoli, A., Oldfield, M., 2020. An adaptive finite element model for steerable needles. Biomechanics and Modeling in Mechanobiology 19, 1809–1825. doi:10.1007/s10237-020-01310-x.

Terzano, M., Spagnoli, A., Ståhle, P., 2018. A fracture mechanics model to study indentation cutting. Fatigue & Fracture of Engineering Materials and Structures 41, 821–830. doi:10.1111/ffe.12750.

Tønnesen, J., Inavalli, V.K., Nägerl, U.V., 2018. Super-Resolution Imaging of the Extracellular Space in Living Brain Tissue. Cell 172, 1108–1121.e15. doi:10.1016/j.cell.2018.02.007.

Vidotto, M., Botnariuc, D., De Momi, E., Dini, D., 2019. A computational fluid dynamics approach to determine white matter permeability. Biomechanics and Modeling in Mechanobiology 18, 1111–1122. doi:10.1007/s10237-019-01131-7.

Wang, X., Hong, W., 2012. A visco-poroelastic theory for polymeric gels. Proceedings of the Royal Society A: Mathematical, Physical and Engineering Sciences 468, 3824–3841. doi:10.1098/rspa.2012.0385.

Zhao, X., 2014. Multi-scale multi-mechanism design of tough hydrogels: building dissipation into stretchy networks. Soft Matter 10, 672–687. doi:10.1039/C3SM52272E.